

Supplemental Data

MAD2-dependent insulin receptor endocytosis regulates metabolic homeostasis

Junhee Park, Catherine Hall, Brandon Hubbard, Traci LaMoia, Rafael Gaspar, Ali Nasiri, Fang Li, Hanrui Zhang, Jiyeon Kim, Rebecca A. Haeusler, Domenico Accili, Gerald I. Shulman, Hongtao Yu, Eunhee Choi

Contents

Figure S1. IR-4A mice show enhanced and prolonged IR signaling.

Figure S2. Metabolic cage studies of male WT and IR-4A mice on normal chow diet.

Figure S3. Insulin signaling and hepatic CEACAM1 levels in WT and IR-4A mice.

Figure S4. The analysis of liver histology and glycogen.

Figure S5. Disruption of IR–MAD2 interaction does not alter the insulin-mediated suppression of lipolysis.

Figure S6. The function of IR–MAD2 interaction in insulin transcytosis.

Figure S7. Metabolomic analysis of plasma samples from WT and IR-4A mice.

Figure S8. Model of the regulation of insulin function by IR–MAD2.

Supplementary Methods

Supplementary References

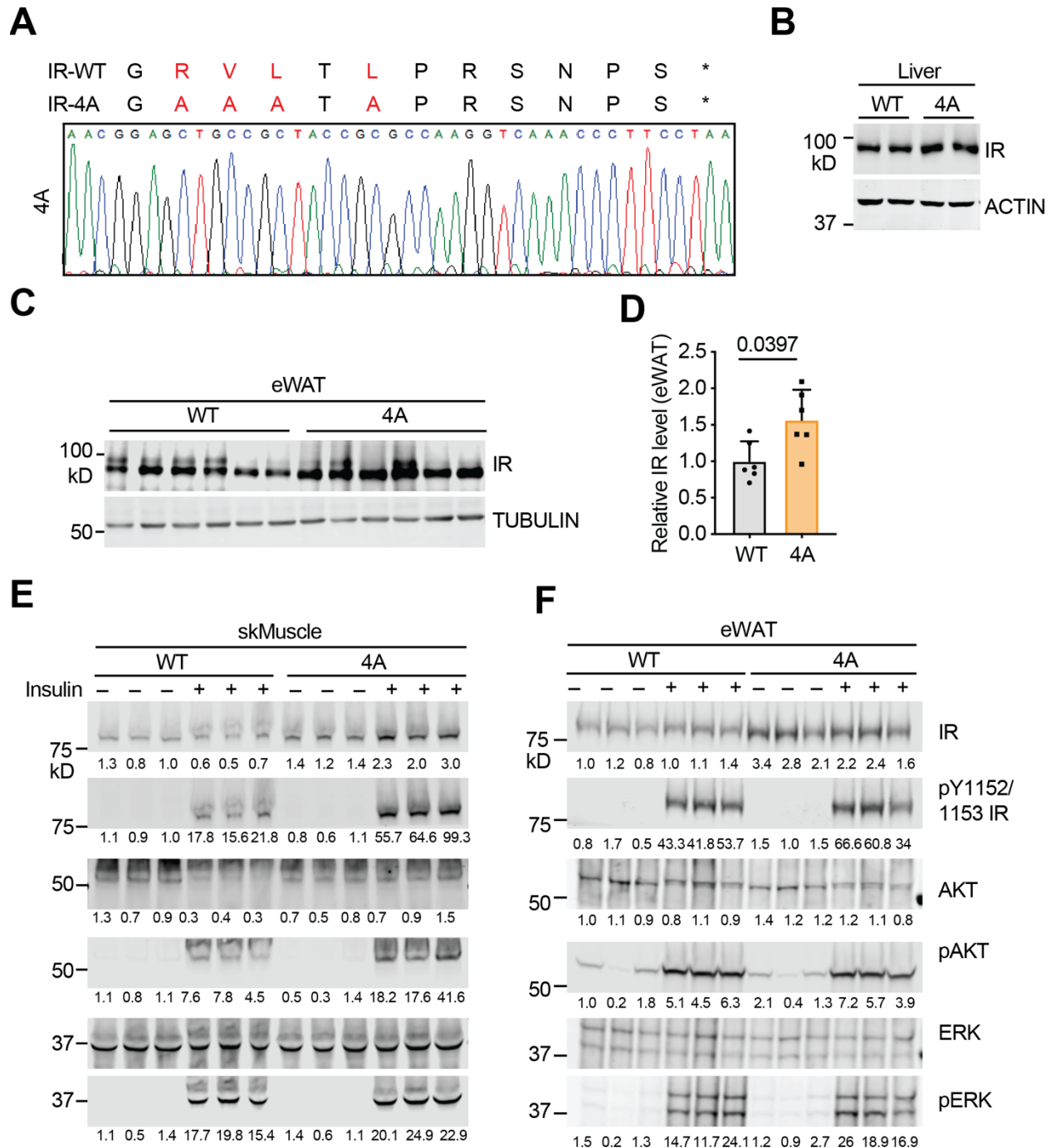


Figure S1. IR-4A mice show enhanced and prolonged IR signaling.

A. Sequencing analysis of genomic DNA from IR-4A mice. WT and IR-4A protein sequences are shown above. The stars (*) indicate stop codon.

B. Representative western blot data of IR levels in the liver from WT and IR-4A mice.

C. IR levels in the eWAT from WT and IR-4A mice.

D. Relative IR levels of eWAT from WT and IR-4A mice in (C). Mean \pm SD. N=6 mice each. Significance calculated using two-tailed student *t-test*.

E. IR signaling in skeletal muscle (skMuscle) lysates of WT and IR-4A mice treated without (-) or with (+) insulin. Each lane contains lysate from an individual mouse. The relative band intensities are quantified, normalized to total ERK, and shown below.

F. IR signaling in eWAT lysates of WT and IR-4A mice treated without (-) or with (+) insulin. Each lane contains lysate from an individual mouse. The relative band intensities are quantified, normalized to total ERK, and shown below.

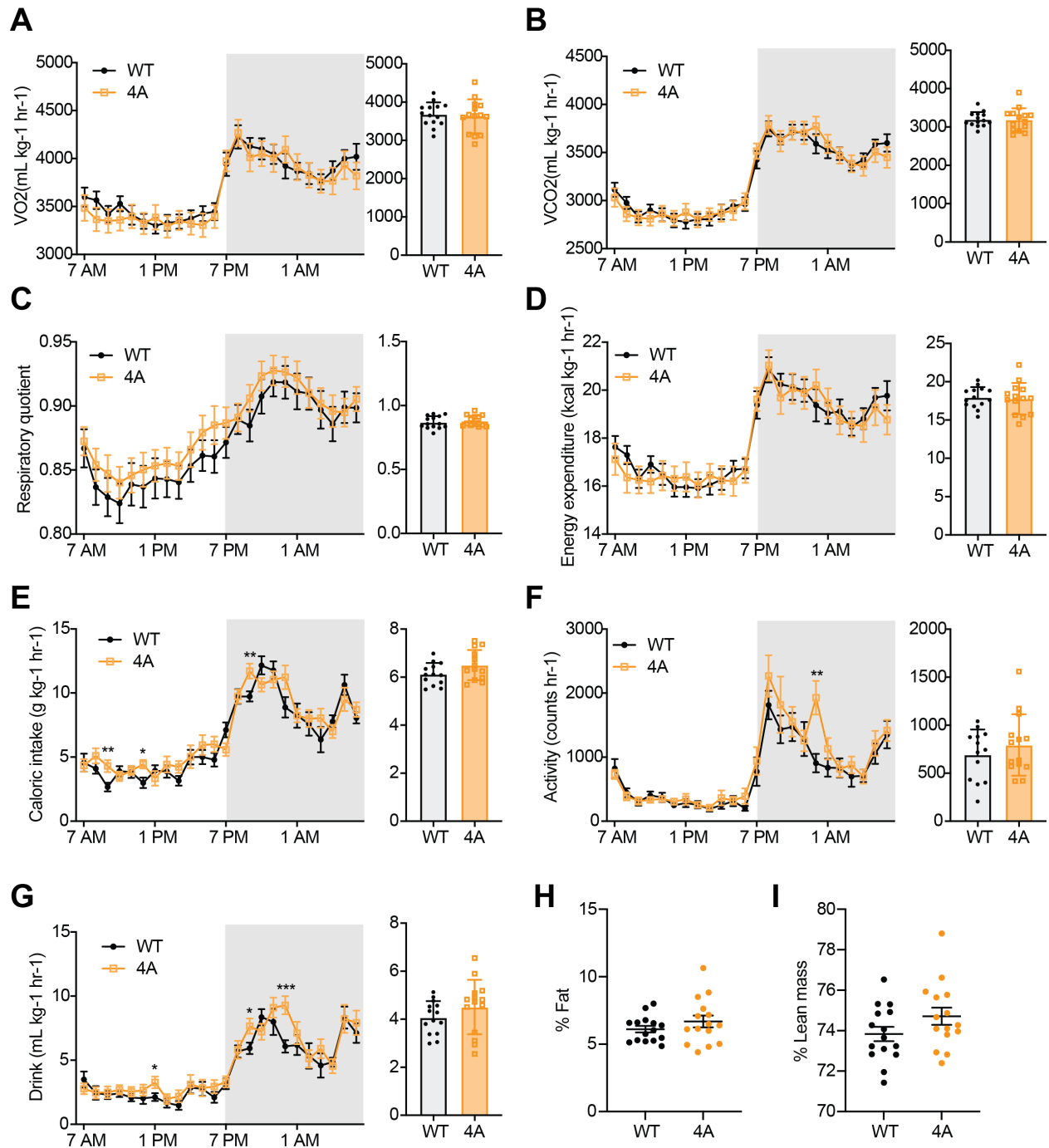


Figure S2. Metabolic cage studies of male WT and IR-4A mice on normal chow diet.

In all panels, data of line graph and scatter dot plot are mean \pm SEM, and data of bar graph are mean \pm SD. N=14 mice each. Significance calculated using two-tailed student *t*-test; **p*<0.05, ***p*<0.01, ****p*<0.001.

A. Oxygen consumption.

B. Carbon dioxide production.

C. Respiratory quotient.

D. Energy expenditure.

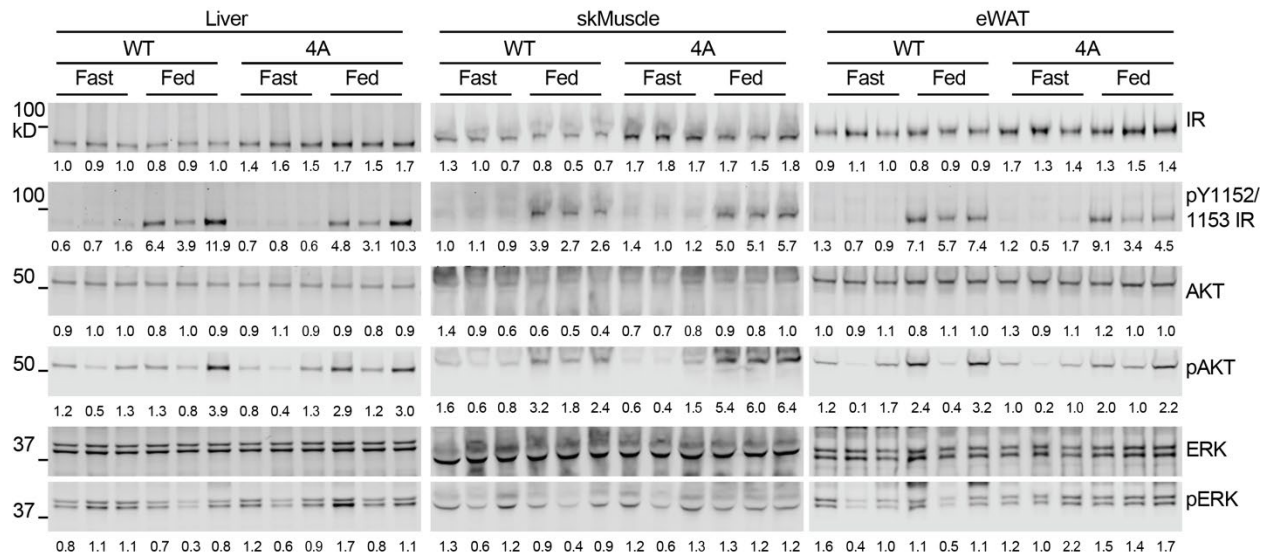
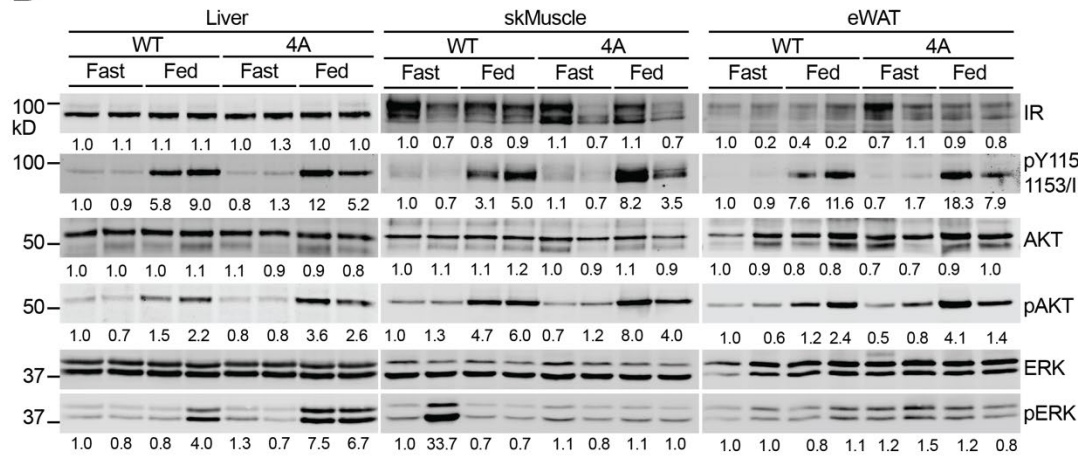
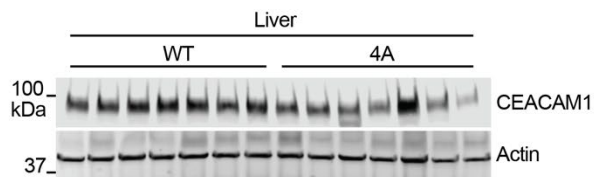
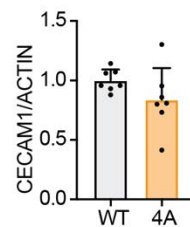
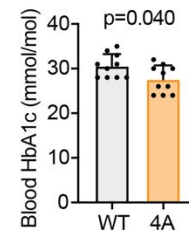
E. Caloric intake.

F. Locomotor activity.

G. Drink.

H. Whole body Fat.

I. Lean mass.

A**B****C****D****E****Figure S3. Insulin signaling and hepatic CEACAM1 levels in WT and IR-4A mice.**

A. IR signaling in liver, skeletal muscle (skMuscle), and eWAT lysates of WT and IR-4A mice after fasting and re-feeding for 2h. Each lane contains lysate from an individual mouse. The relative band intensities are quantified, normalized to total ERK, and shown below.

B. IR signaling in liver, skeletal muscle (skMuscle), and eWAT lysates of WT and IR-4A mice after fasting and re-feeding for 6h. Each lane contains lysate from an individual mouse. The relative band intensities are quantified, normalized to total ERK, and shown below.

C. CEACAM1 levels in the liver from 6h fast WT and IR-4A mice.

D. Quantification of the western blot data shown in (C). Mean \pm SD.

E. Blood HbA1c level in male mice fed HFD for 8 weeks in random feeding conditions from

Figure 5C. Mean \pm SD. N=10 mice each. Significance calculated using two-tailed student *t-test*.

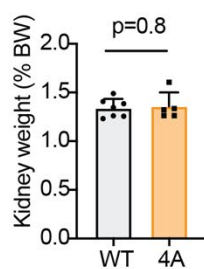
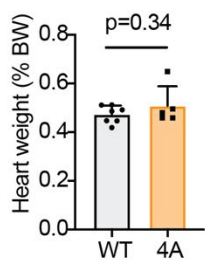
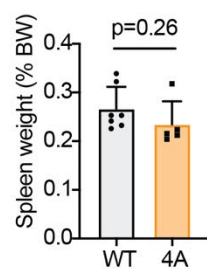
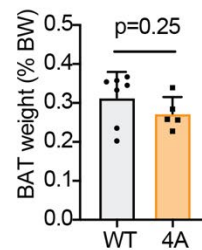
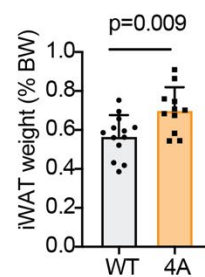
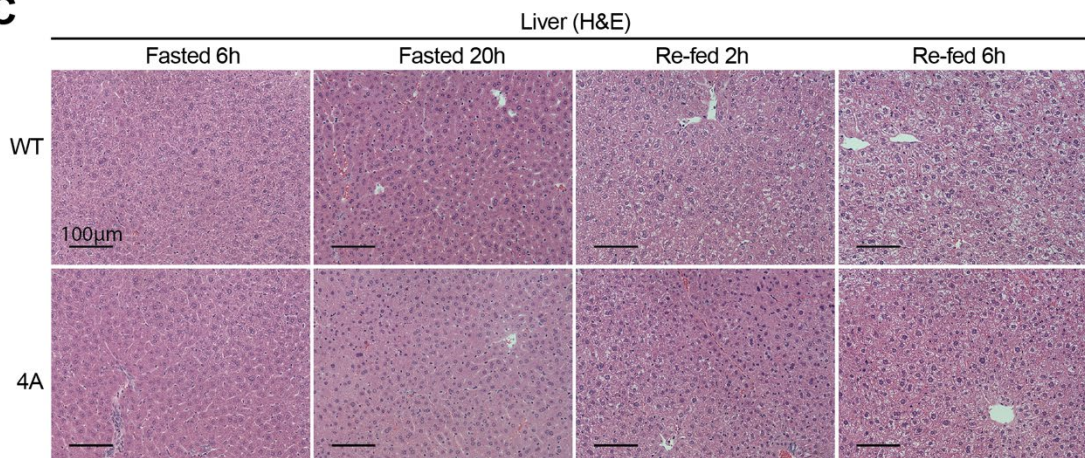
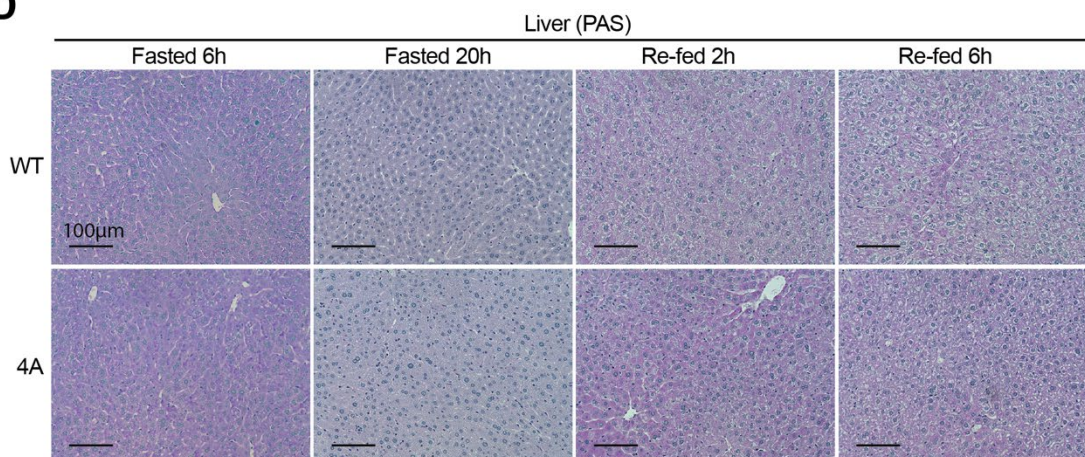
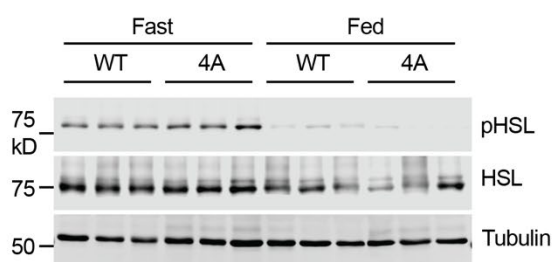
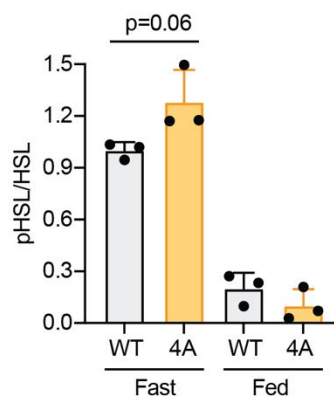
A**B****C****D****E****F**

Figure S4. The analysis of liver histology and glycogen.

A. Spleen, heart, and kidney mass of 20h fasted 2~3-month-old male mice fed normal chow diet. Mean \pm SD. WT N=7; IR-4A, N=5. Significance calculated using two-tailed student *t-test*.

B. inguinal white adipose tissue (iWAT) and intracapsular brown adipose tissue (BAT) mass of 20h fasted 2~3-month-old male mice fed normal chow diet. Mean \pm SD. For inguinal fat, WT, N=13; IR-4A, N=11. For brown fat, WT, N=7; IR-4A, N=5. Significance calculated using two-tailed student *t-test*.

C. Representative H&E staining of livers from WT and IR-4A mice.

D. Representative Periodic acid-Schiff (PAS) staining (magenta) of livers from WT and IR-4A mice.

E. HSL and pHSL levels in the eWAT from 14h fast and 2h re-feeding WT and IR-4A mice.

F. Quantification of the western blot data shown in (E). Mean \pm SD. Significance calculated using two-tailed student *t-test*.

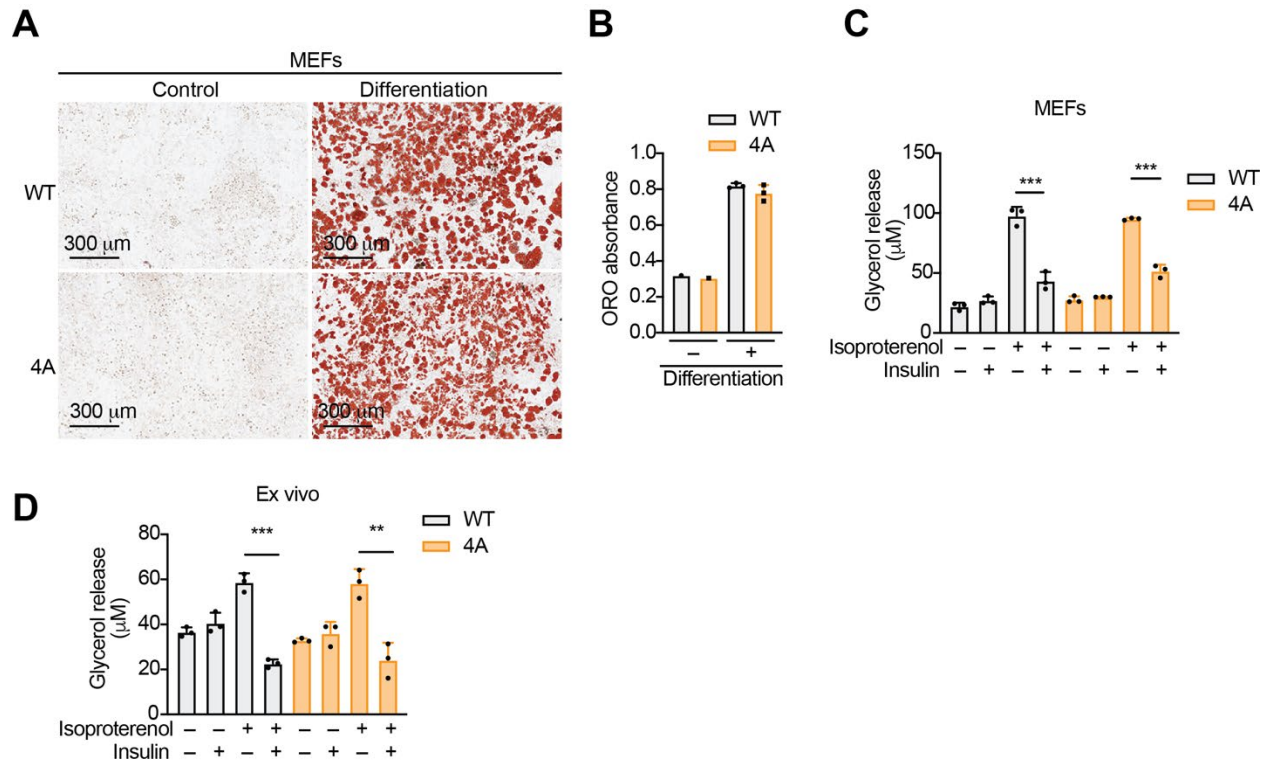


Figure S5. Disruption of IR–MAD2 interaction does not alter the insulin-mediated suppression of lipolysis.

A. Representative images of Oil Red O staining of control and differentiated mouse embryonic fibroblasts (MEFs).

B. Quantification of the Oil Red O staining data shown in (A). Mean \pm SD. Differentiated cells, N=3 each; for differentiated cells, N=1.

C. Glycerol release from adipocyte differentiated MEFs treated without (-) or with (+) 100 nM insulin, and 10 nM isoproterenol. Mean \pm SD. N=3. Significance calculated using two-tailed student *t*-test; *** p <0.001.

D. Glycerol release from ex vivo adipose tissue cultures treated without (-) or with (+) 100 nM insulin, and 10 nM isoproterenol. Mean \pm SD. N=3. Significance calculated using two-tailed student *t*-test; ** p <0.01, *** p <0.001.

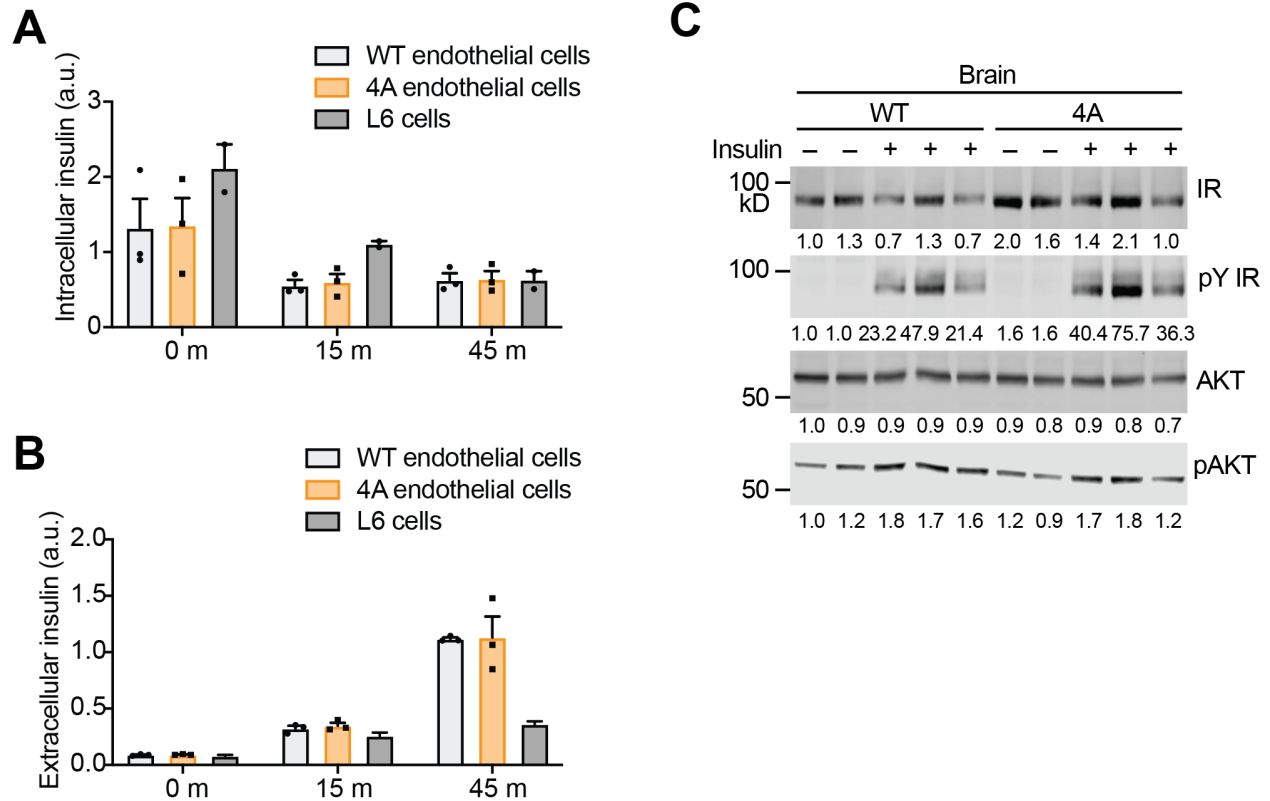
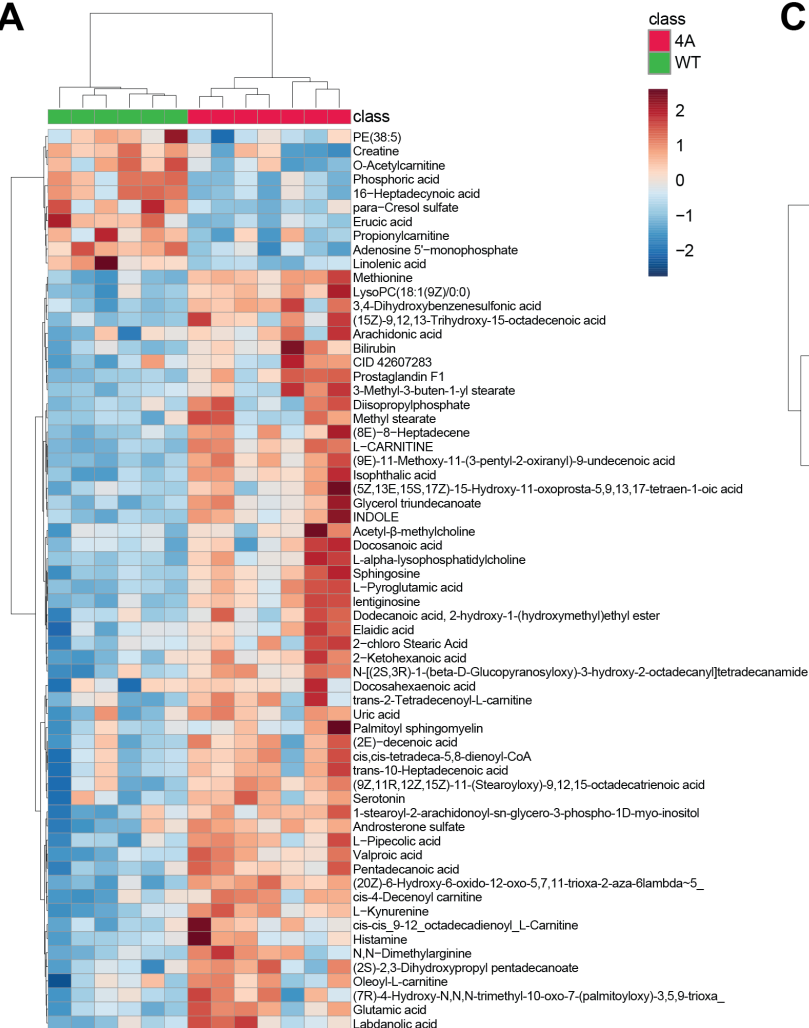


Figure S6. The function of IR–MAD2 interaction in insulin transcytosis.

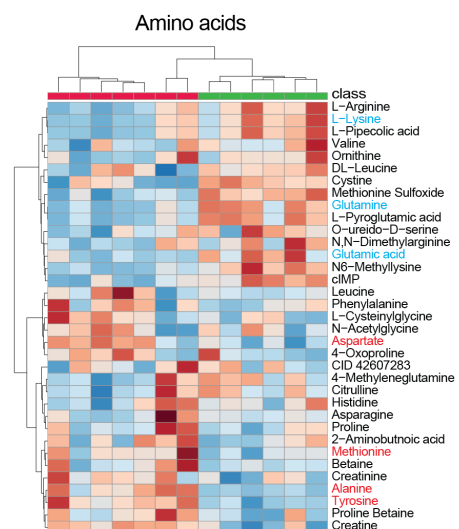
A,B. Levels of intracellular (**A**) and extracellular (secreted) insulin (**B**) of primary endothelial cells and L6 myoblasts after 500 nM insulin treatment for 5 min. Note that due to the detection limit of this assay, we could not further reduce the insulin concentration in the pulse to near physiological concentrations.

C. We measured insulin signaling in the hypothalamus of WT and IR-4A mice after insulin injection via inferior vena cava. Western blots of hypothalamus lysates of WT and IR-4A mice treated without (-) or with (+) insulin. Each lane contains lysate from an individual mouse. The relative band intensities are quantified and shown below.

A



C



B

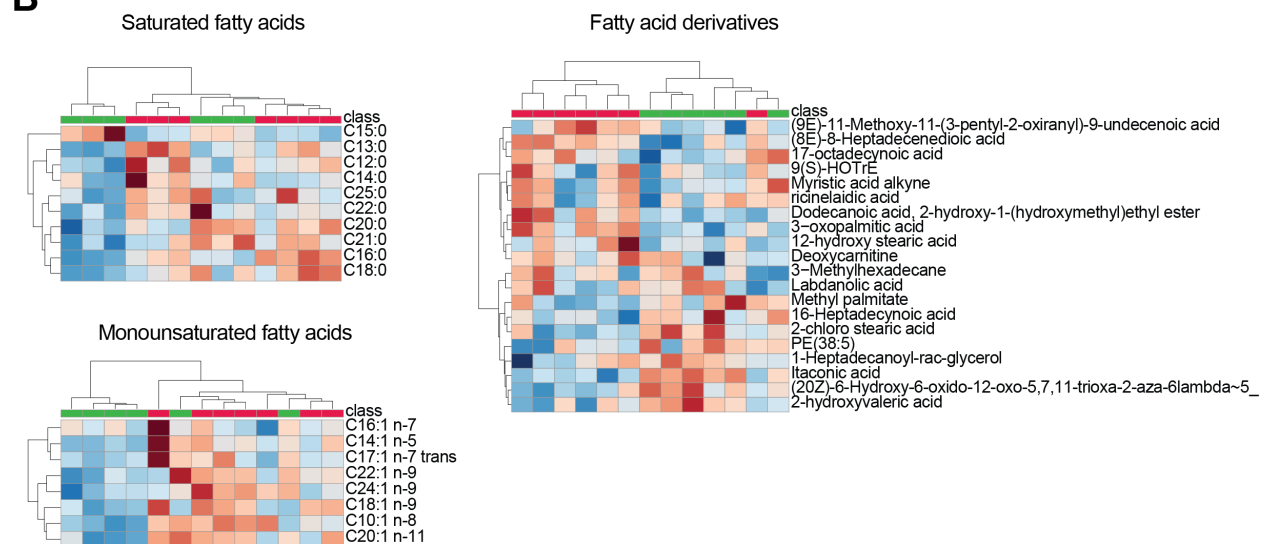


Figure S7. Metabolomic analysis of plasma samples from WT and IR-4A mice.

A. Heat map analysis with hierarchical clustering of identified metabolites in WT and IR-4A plasma samples

B. Heat map of identified saturated fatty acids, monounsaturated fatty acids, and fatty acids derivatives in plasma samples of WT and IR-4A mice.

C. Heat map of identified amino acids in plasma samples of WT and IR-4A mice.

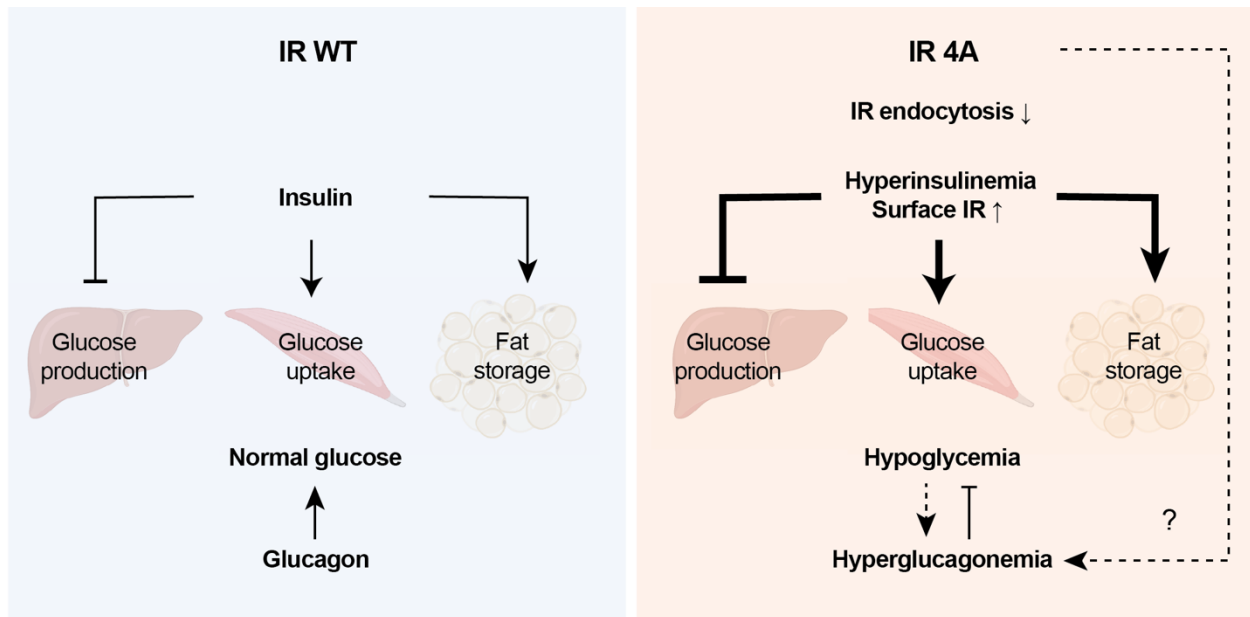


Figure S8. Model of the regulation of insulin function by IR–MAD2.

Disruption of IR–MAD2 interaction delays IR endocytosis and increases basal IR and circulating insulin levels, thus facilitating insulin functions such as glucose uptake and energy storage. In IR-4A mice, mild hypoglycemia or unknown mechanism(s) increase glucose counterregulatory factors, affecting glucose control.

Supplementary Methods

Gene targeting

For targeting Insulin receptor (IR), donor DNA was generated by PCR; Fragment A primers, primer 1 (5'- GTC AAA GCT TCC AGC CTT GAA TAC CAT CTG-3') and primer 2 (5'- AGG AAG GGT TTG ACC TTG GCG CGG TAG CGG CAG CTC CGT TCT TCT TGC CCC CAT-3'); Fragment B primers, primer 3 (5'- ATG GGG GCA AGA AGA ACG GAG CTG CCG CTA CCG CGC CAA GGT CAA ACC CTT CCT-3') and primer 4 (5'- GTC GTC GAC TAT CTG TAA AAA AGC AGG TAC ATT C). The two fragments were connected by PCR, digested and subcloned into pBS vector. A mixture of donor circular DNA (15 ng), Cas9mRNA (100 ng), and sgRNA (75 ng, CCC TAT ACC CAC ATG AAT GGG GG) was microinjected into B6SJLF1/J mouse fertilized eggs. The embryos were transferred to pseudo-pregnant CD1 females. The produced F0 pups were screened by PCR with primers: primer 5 (5'- GTC AAC CTG CTC AAG GAT GA-3') and primer 6 (5'- TTT GAC CTT GGC GCG GTA GC-3'). The positive F0 mice were genotyped with PCR primers outside the homologous arms: primer 7 (5'- CAG TCC CCC TAT AAT TGT TGA-3') and primer 8 (5'- GGT TTG ACC TTG GCG CGG TA-3'). The IR-4A allele was confirmed by sequencing with primers: primer 7 and primer 9 (5'- CAG TTT CAC ATC TGG GCA GA-3'). The gene targeting and generation of IR-4A/+ mice were generated by Janelia Farm-Gene Targeting and Transgenics Facility. We obtained 3 germline-transmitted founders in the B6SJF1/J background. IR-4A mice were backcrossed onto the C57BL/6 background (Stock No. 000664, Jackson laboratory) for at least 9 generations. IR-4A mice from all 3 lines survived and did not show discernable differences from wild-type (WT) mice.

Hyperinsulinemic-euglycemic clamp studies

After surgical implantation of an indwelling catheter in the right jugular vein, mice were allowed to recover 1 week prior to clamp experiments. Following an overnight 15h fast, mice were infused with 3-³H-glucose at a rate of 0.05 $\mu\text{Ci}/\text{min}$ for 120 min to determine basal glucose turnover. Next, a primed infusion of insulin and 3-³H-glucose was administered at 7.14 $\text{mU}\cdot\text{kg}^{-1}\cdot\text{min}^{-1}$ and 0.24 $\mu\text{Ci}/\text{min}$, respectively, for 4 min, after which rates were reduced to 2.5 $\text{mU}\cdot\text{kg}^{-1}\cdot\text{min}^{-1}$ insulin and 0.1 $\mu\text{Ci}/\text{min}$ 3-³H -glucose for the remainder of the experiment. Blood was collected via tail massage for plasma glucose, insulin, and tracer levels at set time points during the 140 min infusion

and a variable infusion of 20% dextrose was given to maintain euglycemia. Glucose turnover was calculated as the ratio of the 3-³H-glucose infusion rate to the specific activity of plasma glucose at the end of the basal infusion and during the last 40 min of the hyperinsulinemic-euglycemic clamp study. Hepatic glucose production represents the difference between the glucose infusion rate and the rate of glucose appearance. A 10 µCi bolus injection of ¹⁴C-2-deoxyglucose was given at 85 min to determine tissue-specific glucose uptake, which was calculated from the area under the curve of ¹⁴C-2-deoxyglucose detected in plasma and the tissue content of ¹⁴C-2-deoxyglucose-6-phosphate. Following collection of the final blood sample, mice were anesthetized with an intravenous injection of 150 mg/kg pentobarbital and tissues were harvested and froze with aluminum forceps in liquid nitrogen. All tissues were stored at -80°C until later use.

Comprehensive animal metabolic monitoring system

Comprehensive animal metabolic monitoring system (Columbus Instruments) was used to evaluate O₂ consumption, CO₂ production, energy expenditure, activity, and food consumption. Drinking was assessed by a computer system counting consumed water droplets.

Quantitative PCR

Total RNA was extracted using TRIzol (Invitrogen) and cDNA was then generated using M-MLV reverse transcriptase (Invitrogen) using 1 µg of RNA. qPCR reaction was performed using PowerUp™ SYBR™ Green Master Mix (Thermo Scientific). Real-time PCR was performed in the 7500 Fast Real-Time PCR System (Life Technologies) and expression levels of the indicated genes were calculated using the $\Delta\Delta C_t$ method by the appropriate function of the software using Gapdh as calibrator. The oligos used for qPCR are listed in **Supplementary Table 2**.

Mouse embryonic fibroblast (MEFs) isolation

The MEFs were isolated as described earlier(1). E14.5 embryos were minced with sterile scalpels and incubated with 0.25% trypsin-EDTA for 10 min at 37°C and 5% CO₂ incubator. Fresh 0.25% trypsin-EDTA was added. After 10 min incubation, cells were put into fresh DMEM containing supplemented 10% (v/v) FBS, 2 mM L-glutamine, 55 mM β-mercaptoethanol, and 1% penicillin/streptomycin, and then centrifuged at 290 g for 5 min. After the supernatant was

removed, the cells were resuspended in the DMEM and incubated at 37°C and 5% CO₂ incubator. The medium was changed the next day to remove debris and floating cells.

Adipocyte differentiation and Oil-Red-O staining

MEFs were cultured in the differentiation induction medium(2) [high-glucose DMEM, 1 µM dexamethasone (Sigma), 0.5 mM 3-isobutyl-1-methylxanthine (IBMX; Sigma), 5 µg/ml insulin (sigma), 10 µM troglitazone (Sigma), 20% FBS, and antibiotics] for 3 days and the adipocyte maturation medium (5 µg/ml insulin, 10 µM Troglitazone, 20% FBS, and antibiotics in high-glucose DMEM). After 7-13 days of differentiation, cells were washed with PBS, fixed with 10% formalin at room temperature for 2 h, washed with 60% isopropanol, dried completely, and stained with Oil Red O staining solution (Sigma) at room temperature for 10 min. The dye retained in the cells was eluted using isopropanol, and OD at 520 nm was determined using a spectrophotometer.

Adipose tissue explants

Epididymal adipose tissue was collected, dissected into ~10 mg pieces, and rinsed in warm PBS using 250 µm cell strainer (Thermo Scientific). Then, the adipose tissue explants were weighted and used for lipolysis assay after incubating with serum-free DMEM for 2h.

Lipolysis assay

Differentiated adipocytes or adipose tissue explants were stimulated with 10 mM with or without 100 nM insulin for 6 h in assay buffer (LIP-1-NC-L1; Zen-Bio). The cell culture supernatants were collected and centrifuged at 500g to remove cell debris. Glycerol release was quantified using the LIP-1-NC-L1 lipolysis kit (Zen-Bio) according to the manufacturer's instructions. Glycerol release from adipose tissue explants was normalized with the weight of explants.

***In vitro* transcytosis assay**

Insulin uptake and release from endothelial cells were measured as reported in previous research(3). Briefly, primary human adipose microvascular endothelial cells were purchased from ScienCell (#7200). Endothelial cells were cultured in Endothelial Cell Medium (ScienCell, #1001) in an incubator at 37°C and 5% CO₂. Cells were plated on gelatin-coated culture dish and used within 48h of reaching confluence. L6 myoblasts were purchased from ATCC (CRL-1458™) and

cultured in DMEM supplemented with 10% fetal bovine serum. Cells were treated with or without 500 nM insulin for 5 min at 37°C. The cells were collected in buffer containing 50 mM Tris (pH 8.0), 150 mM NaCl, and 0.25% Triton X-100, and frozen and thawed once. Protein concentration was assessed using Micro BCA Protein Assay Kit (Thermo Scientific). Intracellular and extracellular insulin levels were measured using insulin ELISA kits (Crystal Chem, #90080).

High-resolution metabolomic profiling

Untargeted Metabolomic profiling was conducted using ultrahigh performance liquid chromatography-high resolution accurate mass (HRAM) mass spectrometry (HRAM-MS)(4). Briefly, 50 µL of mouse plasma was mixed with 100 µL of acetonitrile containing a mixture of 9 stable isotope internal standards(5). Sample mixtures were incubated on ice for 30 min, and centrifuged for 10 min at 14 000g at 4 °C to precipitate the proteins. Supernatants were transferred to LCMS vials for analysis.

Ten µL of extracts were analyzed using a high-resolution accurate-mass (HRAM) platform consisting of Vanquish™ UHPLC system equipped with dual split sampler configuration coupled to a Q Exactive HF-X hybrid quadrupole Orbitrap mass spectrometer (Thermo Fisher Scientific, San Jose, CA, USA). Chromatographic separation was performed in triplicate by HILIC chromatography under positive ion mode and RP chromatography under negative ion mode, both at 60°C. HILIC separation was achieved on a Waters XBridge BEH Amide XP column (2.1 mm, 50mm. 2.5 µm) and gradient elution with mobile phases 0.2% formic acid in water (A) and acetonitrile (B). The initial 75% B at 0.35 mL/min kept for 1.5min, decreased linearly to 20% B at 4 min with a flow rate increase to 0.4 mL/min, and a final hold of 1 min. Reverse-phase separation was performed on a C18 column (Higgins Targa C18 2.1 × 50 mm, 3 µm) with 1mM Ammonium acetate in water (solvent A) and Acetonitrile (solvent B). The initial 35% B at 0.4 mL/min, was increased linearly to 95% B at 1.5 min and held for the remaining 3.5 min with a flow rate 0.5 mL/min.

The HRMS was operated in a data dependent (DDA) acquisition mode with resolutions of 60,000 (full scan) and 7500 (dd-MS² scan) in both positive and negative polarity mode to acquire the spectral data. The HRMS source parameters were as follows: spray voltage 3.5 kV (+ESI), 3.00

KV (-ESI); capillary temperature 300 °C; sheath gas flow rate 45; Aux gas 25 AU (+ESI), 15 AU (-ESI); sweep gas flow rate 1 AU; Aux gas heater temperature 250 °C.

The peak area for each detected metabolite was normalized against the total ion count (TIC) of that sample to correct any variations introduced from sample handling through instrument analysis. The normalized areas were used as variables for the multivariate and univariate statistical data analysis. All multivariate analyses and modeling on the normalized data were carried out using MetaboAnalyst v.5.0 (<http://www.metaboanalyst.ca>). Univariate statistical differences in the metabolites between two groups were analyzed using a two-tailed Student's *t-test*. Raw data is provided in **Supplementary Tables 3 and 4**.

RNA sequencing

Total RNA was extracted from liver and adipose tissues using TRIzol (Invitrogen) RNeasy mini kit (Qiagen). All samples were prepared simultaneously to avoid bias related to batched library preparation. Library preparation and RNA sequencing were performed by the Columbia Genome Center. In brief, mRNA was isolated using poly-A tail pulldown and cDNA libraries constructed using TruSeq Stranded mRNA Library Prep Kit (Illumina). Libraries were sequenced using Illumina NovaSeq 6000 at the Columbia Genome Center. Samples were multiplexed in each lane, yielding approximately 20 million 100 bp paired-end reads for each sample.

RNA-seq data processing and Gene Set Enrichment Analysis

Raw sequencing reads were quantified with Salmon v1.8.0 to obtain transcript abundance counts by mapping to mouse genome GRCm39 GENCODE v.M31. The resulting counts were summarized to the gene level using tximport v1.20.0(6). Differential expression was analyzed using DESeq2 v1.32.0(7). Differentially expressed (DE) genes were defined by an absolute fold change > 1.5 and false discovery rate (FDR)-adjusted P value < 0.05 and visualized using Volcano plots. The output of DESeq2 were scored and ranked by apegglm v1.14.0(8) using ranking metrics “ $-\log_{10}$ P value multiplied by the sign of shrunken \log_2 fold-change”(9). The ranked gene list was then subjected to Gene Set Enrichment Analysis (GSEA)(10) to identify the gene sets overrepresented at the top or bottom of the ranked list using pathway definition file “Mouse_GOBP_AllPathways_no_GO_ia_November_17_2022_symbol.gmt” downloaded from

<http://baderlab.org/GeneSets>. Only ontologies with more than 15 genes and less than 200 genes were considered. The top ranked pathways were manually curated to remove the repetitive pathways and visualized using dot plots. The leading-edge genes enriched in the identified pathways were visualized using pheatmap v1.0.12.

Supplementary References

1. Park J, Li J, Mayer JP, Ball KA, Wu J, Hall C, Accili D, Stowell MHB, Bai XC, Choi E: Activation of the insulin receptor by an insulin mimetic peptide. *Nat Commun* 2022;13:5594
2. Choi E, Zhang X, Xing C, Yu H: Mitotic Checkpoint Regulators Control Insulin Signaling and Metabolic Homeostasis. *Cell* 2016;166:567-581
3. Azizi PM, Zyla RE, Guan S, Wang C, Liu J, Bolz SS, Heit B, Klip A, Lee WL: Clathrin-dependent entry and vesicle-mediated exocytosis define insulin transcytosis across microvascular endothelial cells. *Mol Biol Cell* 2015;26:740-750
4. Liu KH, Nellis M, Uppal K, Ma C, Tran V, Liang Y, Walker DI, Jones DP: Reference Standardization for Quantification and Harmonization of Large-Scale Metabolomics. *Anal Chem* 2020;92:8836-8844
5. Soltow QA, Strobel FH, Mansfield KG, Wachtman L, Park Y, Jones DP: High-performance metabolic profiling with dual chromatography-Fourier-transform mass spectrometry (DC-FTMS) for study of the exposome. *Metabolomics* 2013;9:S132-S143
6. Sonesson C, Love MI, Robinson MD: Differential analyses for RNA-seq: transcript-level estimates improve gene-level inferences. *F1000Res* 2015;4:1521
7. Love MI, Huber W, Anders S: Moderated estimation of fold change and dispersion for RNA-seq data with DESeq2. *Genome Biol* 2014;15:550
8. Zhu A, Ibrahim JG, Love MI: Heavy-tailed prior distributions for sequence count data: removing the noise and preserving large differences. *Bioinformatics* 2019;35:2084-2092
9. Reimand J, Isserlin R, Voisin V, Kucera M, Tannus-Lopes C, Rostamianfar A, Wadi L, Meyer M, Wong J, Xu C, Merico D, Bader GD: Pathway enrichment analysis and visualization of omics data using g:Profiler, GSEA, Cytoscape and EnrichmentMap. *Nat Protoc* 2019;14:482-517
10. Subramanian A, Tamayo P, Mootha VK, Mukherjee S, Ebert BL, Gillette MA, Paulovich A, Pomeroy SL, Golub TR, Lander ES, Mesirov JP: Gene set enrichment analysis: a knowledge-based approach for interpreting genome-wide expression profiles. *Proc Natl Acad Sci U S A* 2005;102:15545-15550